Atom abstraction and gas phase dissociation in the interaction of XeF_2 with Si(100)

R. C. Hefty, J. R. Holt, M. R. Tate, and S. T. Ceyer[a)]
Department of Chemistry, Massachusetts Institute of Technology, Cambridge, Massachusetts 02139, USA

(Received 17 July 2008; accepted 22 October 2008; published online 1 December 2008)

Xenon difluoride reacts with Si(100)2×1 by single atom abstraction whereby a dangling bond abstracts a F atom from XeF_2, scattering the complementary XeF product molecule into the gas phase, as observed in a molecular beam surface scattering experiment. Partitioning of the available reaction energy produces sufficient rovibrational excitation in XeF for dissociation of most of the XeF to occur. The resulting F and Xe atoms are shown to arise from the dissociation of gas phase XeF by demonstrating that the angle-resolved velocity distributions of F, Xe, and XeF conserve momentum, energy, and mass. Dissociation occurs within 2 Å of the surface and within a vibrational period of the excited XeF molecule. Approximately an equal amount of the incident XeF_2 is observed to react by two atom abstraction, resulting in adsorption of a second F atom and scattering of a gas phase Xe atom. Two atom abstraction occurs for those XeF product molecules whose bond axes at the transition state are oriented within $\pm60°$ of the normal and with the F end pointed toward the surface. © *2008 American Institute of Physics*. [DOI: 10.1063/1.3025901]

I. INTRODUCTION

Atom abstraction is a mechanism for dissociative chemisorption whereby a bond of a molecule incident upon a surface is cleaved by formation of only a single bond to the surface concomitant with the scattering of the complementary fragment into the gas phase. It has been experimentally identified as the mechanism for the reactions of F_2 (Ref. 1) and XeF_2 (Ref. 2) with Si(100)(2×1). The unambiguous experimental identification of the atom abstraction mechanism for this system was made possible by direct detection of the F or XeF product radical scattered from the surface in a molecular beam-surface scattering ultrahigh vacuum experiment.[3]

In the interaction of XeF_2 with Si(100), a portion of the XeF radical product was also observed to decompose in a collisionless two-body dissociation process during its transit to the triply differentially pumped, rotatable mass spectrometer detector.[2] This experiment showed for the first time that gas phase dissociation of a product of a surface chemical reaction occurs as a result of partitioning of largely the surface reaction exothermicity to vibration of the XeF molecule. The exothermicity of the atom abstraction reaction is quite large. It is calculated to be equal to 67 kcal/mol using a theoretical value (134 kcal/mol) for the F–Si bond energy,[4] a measured value (7 kcal/mol) of the Si–Si π dimer bond energy[5,6] and the F–XeF bond energy. The first F–XeF bond dissociation energy is evaluated to be 60.4 ± 0.5 kcal/mol using spectroscopically determined values for the bond dissociation energy of the Xe–F diatomic molecule, 3.04 ± 0.03 kcal/mol, and the overall dissociation energy of XeF_2, 63.4 ± 0.5 kcal/mol.[7] The total energy available to the reaction products, 69 kcal/mol, is defined as the sum of the exothermicity of the first atom abstraction event and the incident energy of the XeF_2 reactant. The XeF_2 incident energy is equal to the sum of its incident translational energy, 1.4 kcal/mol, plus internal energy, 0.6, or 2 kcal/mol.

This paper is the first of two papers to detail the single F atom abstraction mechanism in the reaction of XeF_2 with Si and the analysis that demonstrates dissociation of XeF via rovibrational excitation in the ground electronic state as a two body, gas phase process. The analysis is based on the demonstration that the angle-resolved velocity distributions of F, Xe, and XeF conserve momentum, energy, and mass. The present work addresses the reaction in the limit of zero fluorine coverage. The second paper addresses this system at higher fluorine coverage.

The present work also addresses a second channel for reaction, two atom abstraction. Two atom abstraction refers to reaction of the XeF product with the Si surface via a second F atom abstraction reaction, resulting in adsorption of both F atoms and production of a gas phase Xe atom. The analysis for gas phase dissociation indicates that two atom abstraction occurs for XeF molecules whose bond axes are oriented within $\pm60°$ of the normal angle and with the F end of XeF pointed toward the surface. These XeF molecules do not escape the strong attractive interaction with the dangling bonds.

This paper is organized as follows. After presentation of the experimental arrangement and the velocity and angular distributions in Secs. II and III, respectively, Sec. IV discusses the dynamics of the intact XeF produced by single F atom abstraction. Section V describes the model for XeF dissociation and compares the simulation results to the data. Section VI discusses the model's assumptions and the physical nature of the dissociation. Section VII analyzes the contribution of the two atom abstraction mechanism to the data

[a)]Electronic mail: stceyer@mit.edu.

presented in Sec. II. Section VIII presents the practical implications of the newly discovered XeF gas phase dissociation mechanism for the chemical etching of Si.

II. EXPERIMENT

A. Experimental procedures

A doubly differentially pumped molecular beam of neat XeF_2 (99+% pure, Lancaster) is incident at $\theta_i=20°$ from the normal angle of a Si(100)(2×1) crystal held at 150 K. The stagnation pressure behind the nozzle orifice is maintained at 0.7 ± 0.1 Torr, which is the vapor pressure of XeF_2 at 298 K. The resulting quasieffusive beam has a measured average kinetic energy of $1.4\pm0.1(\pm2\sigma)$ kcal/mol and an average internal energy of 0.6 kcal/mol, assuming a Boltzmann distribution in the rotational degrees of freedom at 298 K. Accurate analysis of the experimental results requires that the incident XeF_2 beam be uncontaminated with Xe. Therefore, to avoid possible contamination of the beam with free Xe produced by the decomposition of XeF_2, a Teflon® nozzle and gas handling manifold is used. Furthermore, to test for the possible occlusion of Xe gas within the microcrystalline XeF_2 sample, a NMR spectrum is measured.[8] The amount of Xe is found to be below the sensitivity limit of the NMR technique, indicating a maximum of 0.5% of Xe in the XeF_2 reactant.

Time-of-flight (TOF) data are collected at scattering angles of $\theta_d=15°$, 30°, and 60° from the normal angle in the forward scattering direction at each of four masses, $m/e=167$, 148, 19, and 129, corresponding to XeF_2^+, XeF^+, F^+, and Xe^+. The flight-time distribution for each scattered product is measured by a cross-correlation TOF method. A 255 slot pseudorandom chopper disk modulates the stream of scattered particles impinging on the entrance slit of the rotatable, triple differentially pumped, line-of-sight quadrupole mass spectrometer.[3] The rotational frequency of the chopper disk is 392 Hz, resulting in a dwell time of 10 μs per channel. The data are stored in 255 sequential channels. After 571 revolutions of the chopper disk, the data are deconvoluted using the known chopper sequence before each file is saved.

For measurements at $m/e=167$, 148, and 19, the electron energy of the electron impact ionizer is set to 75 eV. For $m/e=129$, it is set to 26.5 eV in order to minimize contributions from dissociative ionization of XeF_2 and XeF.

A Si crystal, determined to be clean by Auger electron spectroscopy (1% detection sensitivity limit) and ordered by He diffraction,[9] is exposed for 4.38 s to the XeF_2 beam, during which TOF data are collected. After exposure, the Si crystal is heated resistively at a rate of 4 K/s to above 1100 K to remove the adsorbed fluorine. This cycle of exposure and heating is repeated until a satisfactory signal-to-noise ratio is attained in the TOF spectrum. In the case of detection of Xe^+ at $m/e=129$, this cycle was repeated between 80 and 160 times at each scattering angle. Given the incident XeF_2 flux of 0.066 ± 0.004 ML F atom/s, a 4.38 s exposure of the Si to XeF_2 results in a coverage range of 0–0.22 ML F atoms. The exposure is calibrated for absolute coverage by comparing the SiF_4 and SiF_2 signals measured in a thermal desorption experiment to those resulting from a known fluorine coverage, 0.94 ± 0.11 ML F atom, as described previously.[9–12]

B. Measurement of the relative transmission of Xe and F

The analysis below requires knowledge of the relative detection sensitivity of Xe and F atoms. One component of the detection sensitivity is the relative transmission probability of Xe and F atoms through the quadrupole field. The procedure for measuring the ratio of transmission functions, T_{129}/T_{19}, has been described in detail previously,[10] so it is summarized briefly here.

Because of the unavailability of a neat beam of F atoms and the negligible change in transmission probability for a unit mass change, the relative transmission probability of Ne is determined. An effusive beam of either pure Ne or Xe, produced by 0.7 ± 0.1 Torr behind the nozzle orifice at room temperature, is directed into the mass spectrometer detector and a TOF spectrum is measured at $m/e=20$ or 129. The velocity-weighted counts of each spectrum are integrated over flight time to yield the flux of each beam, flux^m, where m is the mass. The ratio of the measured flux at each mass is equal to the ratio of absolute flux at each mass, I^m, times the ratio of the electron impact ionization cross section, σ, times the ratio of the transmission probabilities, as given by

$$\left(\frac{\text{flux}^{129}}{\text{flux}^{20}}\right)=\left(\frac{I^{129}}{I^{20}}\right)\left(\frac{\sigma_{Xe\rightarrow Xe^+}}{\sigma_{Ne\rightarrow Ne^+}}\right)\left(\frac{T^{129}}{T^{20}}\right). \quad (1)$$

Since both Xe and Ne beams are effusive and behave as ideal gases, the ratio of their absolute fluxes, I^{129}/I^{20}, is equal to $(m^{20}/m^{129})^{1/2}$. The cross sections for ionization by electron impact, $\sigma_{Xe\rightarrow Xe^+}$ and $\sigma_{Ne\rightarrow Ne^+}$, have been measured.[13] Therefore, the ratio of transmission probabilities, T^{129}/T^{20}, can be calculated and the result is used as the value of T^{129}/T^{19}.

III. EXPERIMENTAL RESULTS AND INITIAL ANALYSIS

A. Scattered TOF at $m/e=167$ XeF_2^+

TOF spectra recorded at $m/e=167$ result exclusively from XeF_2 that is unreactively scattered. Because less than 1% of the incident XeF_2 scatters unreactively from Si over the 0–0.22 ML range of coverage, the XeF_2 signal does not quantitatively affect the analysis of the XeF and Xe TOF spectra. Therefore, the XeF_2 spectra are not shown here. Maxwell–Boltzmann distributions with a temperature of 194 ± 60 K and a flow velocity of 132 ± 44 m/s fit well to these spectra, yielding an average energy and velocity of 1.49 ± 0.07 kcal/mol and 263 ± 6 m/s, respectively.[14]

B. Scattered TOF at $m/e=148$ (XeF^+)

TOF spectra at $m/e=148$ are measured at three scattering angles, $\theta_d=15°$, 30°, and 60°. The spectra at $\theta_d=15°$ and 60° are the result of signal averaging 40, 4.38 s exposures of Si to XeF_2 and the spectrum at $\theta_d=30°$ is the result of averaging 81, 4.38 s exposures. The $m/e=148$ spectra contain contributions not only from the XeF parent species but also

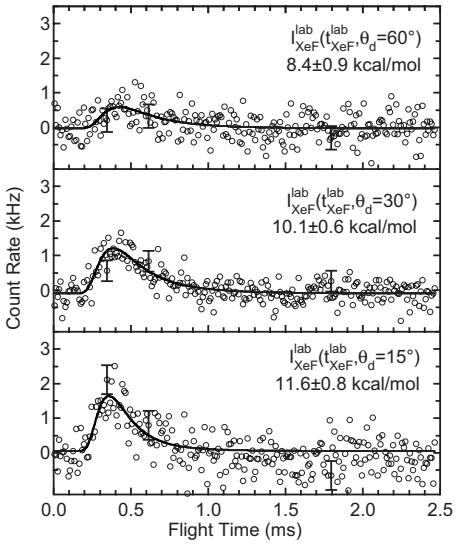

FIG. 1. Net XeF TOF spectra at three scattering angles, θ_d, measured from the normal angle. The line represents fit to Maxwell–Boltzmann distribution, Eq. (2). Average energy and its $\pm 2\sigma$ uncertainty shown.

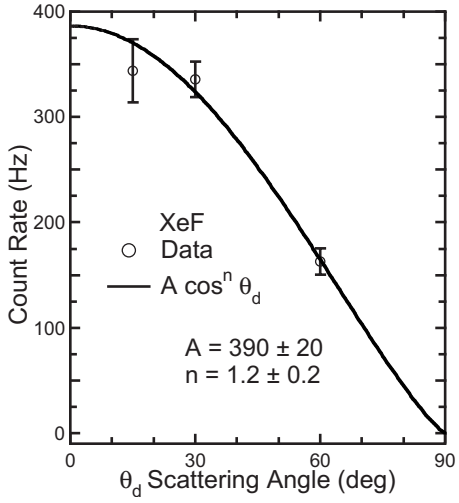

FIG. 2. Angular distribution of XeF flux. Experimental flux determined by time integration of the velocity-weighted counts of the TOF spectrum at each angle in Fig. 1. The line represents fit to Eq. (3).

from dissociative ionization of unreactively scattered XeF_2 upon electron bombardment ionization in the mass spectrometer to form XeF^+. The different velocities with which the XeF species and the XeF_2 molecule scatter from the surface can unambiguously distinguish these contributions.[15] Specifically, the fragmentation ratio, $\sigma_{XeF_2\rightarrow XeF^+}/\sigma_{XeF_2\rightarrow XeF_2^+}$, is determined by directing the incident XeF_2 beam into the detector and measuring the relative signals at $m/e=148$ and 167. The Maxwell–Boltzmann distribution fit to the $m/e=167$ TOF spectrum described above is multiplied by this fragmentation ratio, 1.9/1, and is then subtracted from the corresponding spectrum at $m/e=148$. The resulting spectra, shown in Fig. 1, thus contain no contribution from fragments arising from the dissociative ionization of XeF_2. The error bars represent the propagated statistical uncertainty in the data.[16]

The spectra in Fig. 1 are fit to a Maxwell–Boltzmann distribution function of the form

$$I(t) = A\frac{L^3}{t^4}\exp\left[-\left(\frac{mL^2}{2kT}\right)\left(\frac{1}{t}-\frac{1}{t_f}\right)^2\right] - B, \tag{2}$$

where B is the base line of the background mass spectrometer signal, A is a scaling factor, L is the neutral flight path length from the chopper disk to the ionizer region, k is Boltzmann's constant, T is temperature, t is flight time, and t_f is flow time, which is related to the flow velocity, v_f, as $t_f = L/v_f$. The parameters B, A, T, and t_f are adjusted to achieve the best fit. The fit is shown as a line. The energies displayed in Fig. 1 are the average energies calculated from the fit. The uncertainty in the average energies, defined as 2σ, is also shown.

The angular distribution of scattered XeF is shown in Fig. 2. The flux of XeF at each of three scattering angles, $F(\theta_d)$, is plotted versus scattering angle, θ_d. The flux is determined by the time integration of the velocity-weighted counts of each TOF spectrum in Fig. 1. The $F(\theta_d)$ distribution is then fit to the form

$$F(\theta_d) = A\cos^n\theta_d. \tag{3}$$

The best fit values for A and n are shown in Fig. 2. This angular distribution, which is almost a cosine function, is used in the XeF dissociation simulation discussed below.

C. Scattered TOF at $m/e=19(F^+)$

TOF spectra at $m/e=19$ are measured at three scattering angles, $\theta_d=15°$, 30°, and 60°. The spectra at $\theta_d=15°$ and 60° are the result of signal averaging 40, 4.38 s exposures of Si to XeF_2 and the spectrum at $\theta_d=30°$ is the result of averaging 81, 4.38 s exposures. In addition to neutral F scattered from the surface, the $m/e=19$ spectra contain contributions from both dissociative ionization of unreactively scattered XeF_2 upon electron bombardment ionization to form F^+ and dissociative ionization of XeF to form F^+. The contribution from XeF_2 is determined, as described above for the contribution of XeF_2 to the $m/e=148$ spectra, to be 0.33 ($\sigma_{XeF_2\rightarrow F^+}/\sigma_{XeF_2\rightarrow XeF_2^+}$). The contribution due to dissociative ionization of XeF to form F^+ is determined by estimating the maximum possible contribution to the TOF spectra. The maximum fragmentation ratio, $\sigma_{XeF\rightarrow F^+}/\sigma_{XeF\rightarrow XeF^+}$, is defined to be the largest value that does not produce a negative count rate of F atoms upon subtraction of the XeF contribution from the measured signal at $m/e=19$. This ratio is determined to be 0.4.[2] The Maxwell–Boltzmann fits to spectra at $m/e=167$ and at $m/e=148$ are multiplied by the appropriate fragmentation ratio and then each is subtracted from the spectrum measured at $m/e=19$. The resulting spectra are shown in Fig. 3. The error bars represent the propagated statistical uncertainty of the data. The spectra are fit to a Maxwell–Boltzmann distribution of the form shown in Eq. (1). The fits are shown as dashed lines. The energies displayed in Fig. 3 are the average energies calculated from the fit. The uncertainty in the average energies, defined as 2σ, is also shown.

Comparison of F atom TOF spectra in Fig. 3 to XeF spectra in Fig. 1 reveals that the spectra are very different. The maximum of the F atom spectrum is clearly at shorter

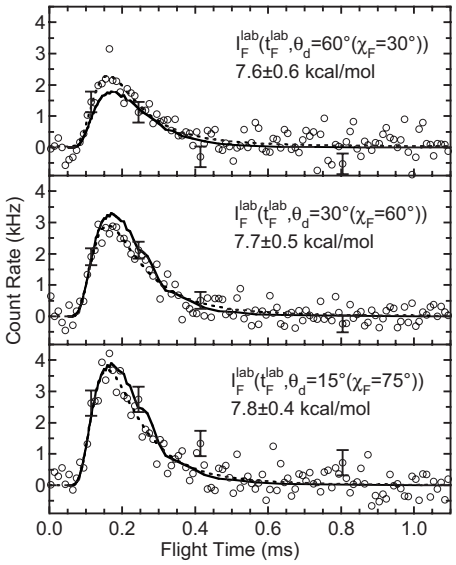

FIG. 3. Net F atom TOF spectra (as described in text) at three scattering angles, θ_d, measured from the normal angle. The dashed line is fit to Maxwell–Boltzmann distribution, Eq. (2). Average energy and its $\pm 2\sigma$ uncertainty shown. The solid line represents simulated result, Eq. (10).

times than that of the XeF spectrum. This difference unambiguously shows that F atoms are produced via a different mechanism than XeF fragments and that F atoms do not arise from dissociative ionization of XeF in the detector.

The angular distribution of scattered F is shown in Fig. 4. The flux of F at each of three scattering angles, F(θ_d), is plotted versus scattering angle, θ_d. The flux is determined by the time integration of the velocity-weighted counts of the TOF spectrum at each angle in Fig. 3.

D. Scattered TOF at $m/e=129$(Xe^+)

TOF spectra at $m/e=129$ are measured at three scattering angles, $\theta_d=15°$, 30°, and 60°. The spectrum at $\theta_d=15°$ is the result of signal averaging 80, 4.38 s exposures of the Si to XeF_2 and spectra at $\theta_d=30°$ and 60° are the result of averaging 160, 4.38 s exposures at each scattering angle. In

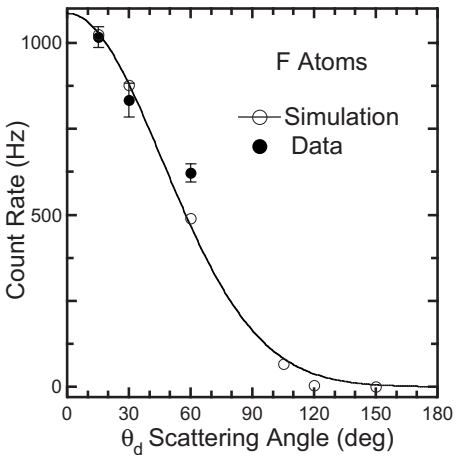

FIG. 4. Angular distribution of F flux. The solid dots represent experimental flux determined by time integration of the velocity-weighted counts of the TOF spectrum at each angle in Fig. 3. Open dots represent simulated fluxes. Line represents fit to simulated flux, Eq. (14).

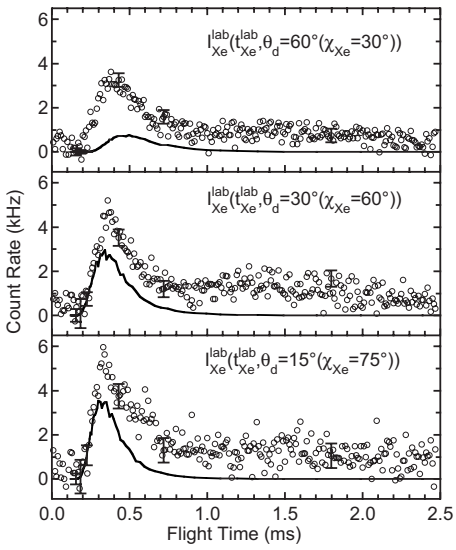

FIG. 5. Net Xe atom TOF spectra at three scattering angles, θ_d, measured from the normal angle. Line represents simulated result, Eq. (10).

addition to neutral Xe scattered from the surface, $m/e=129$ spectra contain contributions from both dissociative ionization of unreactively scattered XeF_2 upon electron bombardment ionization in the mass spectrometer to form Xe^+ and dissociative ionization of XeF to form Xe^+. The contribution from XeF_2 is determined, as described above for the contribution of XeF_2 to the $m/e=148$ spectra, to be 0.045 ($\sigma_{XeF_2\rightarrow Xe^+}/\sigma_{XeF_2\rightarrow XeF_2^+}$). The contribution due to dissociative ionization of XeF to form Xe^+ is determined to be 1 ($\sigma_{XeF\rightarrow Xe^+}/\sigma_{XeF\rightarrow XeF^+}$) by estimating the maximum possible contribution to the TOF spectra that results in non-negative signal intensity, as described above for the dissociative ionization contribution of XeF to form F^+. However, spectra measured at coverages greater than 0.22 ML are inconsistent with this large fragmentation ratio and indicate that the value of this fragmentation ratio, $\sigma_{XeF\rightarrow Xe^+}/\sigma_{XeF\rightarrow XeF^+}$, is closer to 0.5.[14,17] Therefore, the fragmentation value of 0.5 is used here. The conclusions presented below are independent of the value of this fragmentation ratio over the range 0 to 1. The Maxwell–Boltzmann fits to the spectra at $m/e=167$ and $m/e=148$ are multiplied by the appropriate fragmentation ratio and then each is subtracted from the spectrum measured at $m/e=129$. The resulting spectra are shown in Fig. 5. The error bars represent the propagated statistical uncertainty of the data.

IV. OBSERVATION AND DYNAMICS OF ATOM ABSTRACTION

The detection of molecular XeF scattered from the surface, as observed in Fig. 1, is clear evidence for the atom abstraction reaction channel. Previous work concluded that for fluorine coverages below about 1 ML, the dangling bonds are not only the fluorine adsorption sites upon interaction of XeF_2 and F_2 with Si(100)2×1, but that they are also the abstraction sites.[9] Therefore, as XeF_2 approaches the surface, a dangling bond abstracts one of the F atoms, while the complementary XeF fragment is scattered away from the surface. The spectra in Fig. 1, measured at a Si temperature of

150 K and an incident XeF_2 energy and angle of 1.4 kcal/mol and 20°, respectively, show that the average translational energy of XeF varies between 8.4 and 11.6 kcal/mol, depending on the scattering angle.

The relatively high translational energies of the scattered XeF, 8.4–11.6 kcal/mol, as well as the dependence of the translational energy on scattering angle indicate that XeF does not remain on the surface after the abstraction reaction and equilibrate with it. Had the XeF fragment equilibrated and desorbed from the surface, its average translational energy would have been equal to $2kT$ or 0.60 kcal/mol, where T is the Si temperature, 150 K, and its translational energy would have been independent of scattering angle. Therefore, the independence of the XeF product translational energy on Si temperature demonstrates that the XeF translational energy is determined solely by the dynamics of the atom abstraction reaction. This conclusion is supported by additional measurements, not shown here, of the translational energies of XeF produced upon the abstraction reaction of XeF_2 with Si(100) at 250 K, for $\theta_i=30°$ and for a range of incident energies up to 6.3 kcal/mol (Ref. 18) that reveal similarly high translational energies that depend on the scattering angle. The independence of the scattered XeF angular and energy distributions on the incident angle and incident energy, as well as surface temperature, is consistent with the presence of strong chemical forces at the surface. These forces eliminate memory of the initial state of XeF_2.

The observed values of translational energies indicate that between 12% and 17% of the 69 kcal/mol energy available to the abstraction reaction is channeled into translational degrees of freedom of the XeF product. The small percentage of available energy partitioned into translation is consistent with an "early barrier" or "attractive" type of potential energy surface first described by Evans and Polanyi[19] for gas phase reactions. In the prototypical three atom reaction $A+BC \rightarrow AB+C$, an "attractive potential" surface leads to high vibrational energy in AB and to low translational energy in the products AB and C. For the gas-surface case of XeF_2 on Si(100), where A is the Si surface atom with its dangling bond, B is F, and C is XeF, the vibrational excitation is in the surface Si–F bond. Emission observed at about 1400 cm^{-1} during exposure of XeF_2 to polycrystalline Si has been attributed to the decay of such a vibrationally excited fluorinated Si surface species.[20]

While the percentage of exothermicity partitioned into translation is small, it is larger than that observed for F atom abstraction from F_2, which has been measured as 4% for an incident energy of 0.7 kcal/mol. For similar incident energies and relative masses of A, B, and C, the percentage of exothermicity partitioned into translation is inversely related to the strength of the attractiveness of the potential energy surface. Given that the F atom abstraction reaction from F_2 or XeF_2 by a Si dangling bond is essentially a barrierless reaction, the attractiveness of the potential energy surface is determined largely by reaction exothermicity. Therefore, because abstraction of F from XeF_2 is less exothermic than abstraction from F_2 by about 23 kcal/mol, the larger percentage of exothermicity partitioned to translation in the XeF_2 abstraction reaction is expected. However, the larger percentage is likely less than expected based on the attractiveness of the potential surface because in the XeF_2 reaction, the complementary fragment, XeF, is heavy compared to the complementary F atom in the F_2 reaction. This mass difference affects the kinematics so that the efficiency of conversion of the exothermicity to vibration is greater in the XeF_2 abstraction than in the F_2 abstraction reaction, if the reaction is strictly collinear.[21]

It is doubtful that the transition state of the abstraction reaction is collinear (that is, the Si, F and XeF atoms or fragments lie on a line). The XeF angular distributions measured under all initial conditions and surface temperatures in the limit of zero coverage are observed to follow an almost cosine function around the normal. The near cosine dependence of the XeF scattered flux with angle is indicative of a floppy transition state that results in scattering of the product over a wide range of angles. This experimental evidence indicates that the transition state is noncollinear, and hence, makes the prediction about mass effects on the kinematics uncertain.

V. XeF DISSOCIATION MODEL

A. Description of model

The observation of F atoms suggests that dissociation of XeF occurs in the gas phase, after the XeF molecules leave the surface and prior to reaching the detector. Dissociation results from some of the 69 kcal/mol energy available to the abstraction reaction being channeled into internal excitation of the scattered XeF molecule. If this excitation is greater than the XeF bond energy, 3 kcal/mol,[7] XeF can decompose. The internal energy above the dissociation energy is converted to translational energy of the F and Xe atoms moving away from each other in opposite directions in the center-of-mass frame.

A model is developed to test the hypothesis that the F atoms arise from gas phase dissociation of the product of a surface chemical reaction, XeF. The model predicts the Xe atom velocity and angular distributions by applying the laws of conservation of momentum, energy, and mass to the measured F and XeF velocity and angular distributions. The predictions for Xe must agree with the measured Xe velocity and angular distributions if the XeF dissociation is a two-body, gas phase event, without the involvement of the surface as a third body.

The conservation of momentum and energy relationships in the center-of-mass frame are defined by

$$m_{Xe}\vec{v}_{Xe}^{cm} = -m_F\vec{v}_F^{cm} \tag{4}$$

$$\tfrac{1}{2}m_{Xe}|\vec{v}_{Xe}^{cm}|^2 + \tfrac{1}{2}m_F|\vec{v}_F^{cm}|^2 = E_{int}(XeF) - E_{diss}(XeF) = E_{cm}, \tag{5}$$

where m is the mass and $\vec{v}_F^{cm}$ is the center-of-mass velocity of the designated species, E_{int} is the available energy channeled into XeF internal energy, and E_{diss} is the XeF bond dissociation energy. Equation (4) states that the momentum of the Xe atom must be equal to but opposite in direction to the momentum of the F atom in the center-of-mass frame. Equation (5) sets the sum of translational energies of the F and Xe

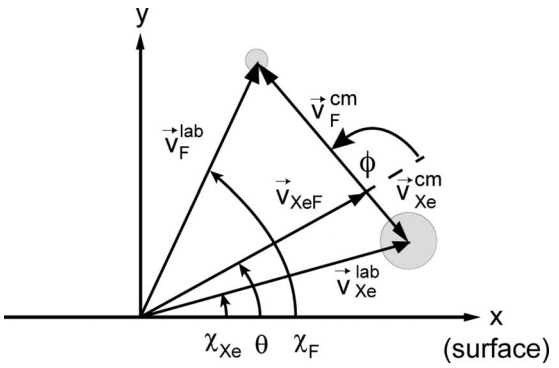

FIG. 6. Newton diagram relating center-of-mass and laboratory frame velocity vectors for gas phase dissociation of XeF.

atoms equal to the difference between the available reaction energy partitioned to the XeF internal degrees of freedom, E_{int}(XeF), and the XeF bond dissociation energy, E_{diss}(XeF). This difference is defined as E_{cm}, which is the XeF internal energy that is converted to translational energy of the Xe and F atoms upon XeF dissociation. Solving Eqs. (4) and (5) for the center-of-mass velocities yields

$$|\vec{v}_F^{cm}| = \sqrt{\frac{2E_{cm}}{m_F\left(1+\frac{m_F}{m_{Xe}}\right)}} \quad |\vec{v}_{Xe}^{cm}| = \sqrt{\frac{2E_{cm}}{m_{Xe}\left(1+\frac{m_{Xe}}{m_F}\right)}}. \tag{6}$$

The magnitude of the center-of-mass velocities depends solely on E_{cm} and the F and Xe masses. Because $\vec{v}_F^{cm}$ is derived from the measured F atom TOF spectra, E_{cm} can be calculated from the first equality in Eq. (6). In turn, E_{cm} is used in the second equality in Eq. (6) to predict $\vec{v}_{Xe}^{cm}$ and those predictions are compared to the measured Xe atom TOF spectra. If dissociation of XeF is a gas phase process, then the predicted Xe spectra must agree well with those measured.

However, because XeF is moving away from the surface during the dissociation event, and because the F, Xe, and XeF TOF distributions are measured in the laboratory frame, it is necessary to add the center-of-mass velocity vectors of the resulting F and Xe atoms to the velocity vector of XeF, as illustrated in the Newton diagram in Fig. 6 before a comparison between the predictions and the measured velocities can be made. Using the illustrated vector addition, the F and Xe laboratory frame velocities are

$$\vec{v}_F^{lab} = \vec{v}_{XeF} + \vec{v}_F^{cm} \quad \vec{v}_{Xe}^{lab} = \vec{v}_{XeF} + \vec{v}_{Xe}^{cm}, \tag{7}$$

where $\vec{v}_{XeF}$ is the laboratory frame velocity vector of XeF. Figure 6 also illustrates the definition of θ as the scattering angle of XeF with respect to the surface plane (where $\theta = 90° - \theta_d$ in Fig. 1), of χ_F and χ_{Xe} as the scattering angles of F and Xe with respect to the surface plane, respectively (where $\chi_F = 90° - \theta_d$ in Fig. 3 and $\chi_{Xe} = 90° - \theta_d$ in Fig. 5) and of ϕ as the XeF bond axis orientation with respect to $\vec{v}_{XeF}$. It is clear from Fig. 6 that the F laboratory velocity is determined by the XeF scattering angle θ, the F scattering angle χ_F, and the XeF bond axis orientation ϕ. Note also that the measured F laboratory velocities and scattering angles are distributions of velocities and angles, $I_F^{lab}(v_F^{lab}, \chi_F)$. The distributions arise because there is a distribution of reaction exothermicities and incident energies partitioned to the internal degrees of freedom of the XeF product and hence, a distribution of values of E_{cm}, denoted as $I(E_{cm})$. In addition, there is a distribution of XeF bond axis orientations when XeF dissociates, denoted as $I(\phi)$, as well as a distribution of velocities and scattering angles of the dissociating XeF.

The procedure to determine $I(E_{cm})$ and $I(\phi)$ is as follows. The flux distribution of F atom laboratory velocities, $I_F^{lab}(v_F^{lab}, \chi_F)$, which is measured as a number density TOF spectrum at various laboratory scattering angles shown in Fig. 3, is related to the equivalent distribution[15] in the center-of-mass system, $I_F^{cm}(v_F^{cm}, \phi)$ by the geometrical Jacobian $(v^{lab}/v^{cm})^2$,

$$I_F^{lab}(v_F^{lab}(v_{XeF}), \chi_F(\theta)) = \left(\frac{v_F^{lab}}{v_F^{cm}}\right)^2 I_F^{cm}(v_F^{cm}(E_{cm}), \phi) \propto \frac{(v_F^{lab})^2}{v_F^{cm}} I(E_{cm}) I(\phi). \tag{8}$$

The proportionality in Eq. (8) relates the center-of-mass velocity distribution to an energy distribution via the Jacobian v^{cm} and shows the center-of-mass energy distribution, $I_F^{cm}(E_{cm}, \phi)$, approximated as the product of $I(\phi)$, the probability that XeF dissociates at axis orientation ϕ, and $I(E_{cm})$.[15] Thus, the laboratory frame velocities and scattering angles of F (and Xe) atoms resulting from gas phase dissociation of XeF following an abstraction event are determined from knowledge of the laboratory frame XeF velocity, $\vec{v}_{XeF}$, the scattering angle, θ, of XeF from the Si surface, the orientation of the XeF bond axis, ϕ, with respect to $\vec{v}_{XeF}$, and the center-of-mass velocities, $\vec{v}_F^{cm}$ (and $\vec{v}_{Xe}^{cm}$).

Strictly speaking, the laboratory frame velocity and angular distributions of the dissociating XeF are not known because they cannot be measured. Rather, the velocity and angular distributions for intact XeF reaching the detector are measured, as shown in Figs. 1 and 2, and are used to represent the distributions of XeF that undergo dissociation in this experiment. The validity of this approximation is discussed below.

The distributions $I(E_{cm})$ and $I(\phi)$ are determined by finding the distributions that best fit the measured F atom TOF distributions in Fig. 3. This aim is accomplished by a forward convolution calculation using Eq. (8), the left hand equalities in Eqs. (6) and (7), the Newton diagram in Fig. 6 and the measured XeF velocity and angular distributions shown in Figs. 1 and 2 to predict $I_F^{lab}(v_F^{lab}, \chi_F)$, the laboratory velocity distribution of the F atom flux at some scattering angle. The velocity distribution in turn is transformed into a number density distribution in time that is compared directly with the TOF spectrum in Fig. 3. The functional forms of $I(E_{cm})$ and $I(\phi)$ or each of their single parameters are adjusted and the forward convolution calculation is carried out iteratively until good agreement is attained. Variation in these two distributions is not entirely decoupled, as discussed in more detail below.

Once the distributions for $I(E_{cm})$ and I(ϕ) are found that

best fit the F atom spectra, they are used to predict $I_{Xe}^{lab}(v_{Xe}^{lab}, \chi_{Xe})$ using Eq. (9), which is the Xe analog to Eq. (8),

$$I_{Xe}^{lab}(v_{Xe}^{lab}(v_{XeF}), \chi_{Xe}(\theta)) = \left(\frac{v_{Xe}^{lab}}{v_{Xe}^{cm}}\right)^2 I_{Xe}^{cm}(v_{Xe}^{cm}(E_{cm}), \phi)$$
$$\propto \frac{(v_{Xe}^{lab})^2}{v_{Xe}^{cm}} I(E_{cm}) I(\phi), \quad (9)$$

the right hand equalities in Eqs. (6) and (7), the Newton diagram in Fig. 6 and the measured XeF velocity and angular distributions shown in Figs. 1 and 2. The predicted Xe atom velocity distribution, in turn, is transformed into a number density distribution in time that is compared directly to the measured Xe TOF spectra shown in Fig. 5. If dissociation of XeF occurs in the gas phase as a two-body process unperturbed by the surface, then the predicted Xe TOF spectra must agree well with the measured spectra.

In practice, the simulated velocity and angular distributions, $I_F^{lab}(v_F^{lab}, \chi_F)$, are determined by summing of a large number of calculated trajectories. Each trajectory has a specific set of initial conditions given by $\{\phi, \theta, v_{XeF}, E_{cm}\}$. Specifically, 25 discrete values are used for θ, 33 values for ϕ, 70 values for v_{XeF}, and 140 values for E_{cm}. Thus, the resulting simulation matrix contains $25 \times 33 \times 70 \times 140 = 8\,085\,000$ initial trajectories for each of the three scattering angles at which F (or Xe) atom TOF spectra are measured. Each element in this matrix represents a single F (or Xe) atom trajectory resulting from a specific set of initial conditions of the XeF scattering from the surface. The outcome of each F (or Xe) atom trajectory is given by

$$I_{F\ or\ Xe}^{lab}(v_{F\ or\ Xe}^{lab}(v_{XeF}), \chi_{F\ or\ Xe}(\theta))$$
$$= \left(\frac{v_{F\ or\ Xe}^{lab}}{v_{F\ or\ Xe}^{cm}}\right)^2 I(\phi) P(\theta, v_{XeF}) P(v_{F\ or\ Xe}^{cm}), \quad (10)$$

where $P(\theta, v_{XeF})$ is the velocity distribution of XeF at a laboratory scattering angle θ, and $P(v_{F\ or\ Xe}^{cm})$ is the F (or Xe) atom center-of-mass velocity distribution that is related to $I(E_{cm})$ by a Jacobian. An acceptance angle of 3.52°, centered at each of the three scattering angles, is used to reflect the detector configuration.

B. Model results

1. Simulated F atom TOF

The energy distribution, $I(E_{cm})$, arising from the partitioning of the available reaction energy to internal energy above the dissociation energy of XeF is determined by an iterative procedure described above. That is, the functional form of $I(E_{cm})$ and/or its single parameter are varied until the distribution determined by the sum of about 8×10^6 trajectories, each calculated by Eq. (10), matches well the measured F atom spectra. The functional form of the energy distribution $I(E_{cm})$ in the center-of-mass frame that yields the best fit to the F atom data in the limit of zero coverage, 0–0.22 ML is

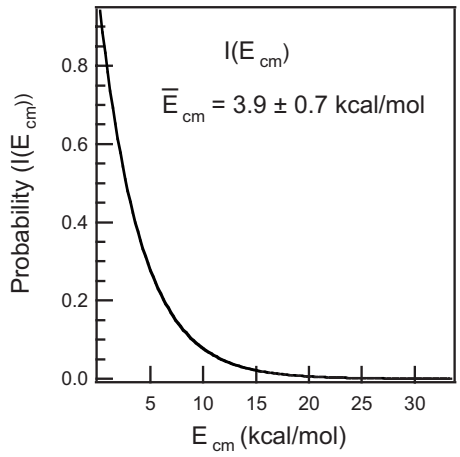

FIG. 7. The energy distribution, $I(E_{cm}) = (RT)^{-1} \exp(-E_{cm}/RT)$, arising from the partitioning of the available reaction energy to internal energy above the XeF dissociation energy that yields the best fit to the F atom TOF spectra. The average energy is shown.

$$I(E_{cm}) = (RT)^{-1} \exp(-E_{cm}/RT). \quad (11)$$

Other forms that were investigated include $I(E_{cm}) \propto E_{cm}^{-1/2} \exp(-E_{cm}/RT)$ and $I(E_{cm}) \propto E_{cm}^{1/2} \exp(-E_{cm}/RT)$, but they yielded simulated TOF spectra that were in visibly poorer agreement with the data. The single exponential decay function is similar to those used previously to describe gas phase dissociation events.[22] The functional form in Eq. (11) was optimized by varying the average energy, $\bar{E}_{cm}$, which is equal to RT. The value of $\bar{E}_{cm}$ that yields the best fit to the measured F atom TOF and angular distributions is 3.9 ± 0.7 kcal/mol, where $T = 1970$ K, as shown in more detail below. A plot of $I(E_{cm})$ is shown in Fig. 7.

The distribution of molecular orientations of the XeF bond axis relative to the velocity vector of XeF, $I(\phi)$, is determined by a similar iterative procedure. As shown in the Newton diagram in Fig. 6, ϕ is defined as the angle between the XeF velocity vector and the XeF molecular axis. However, for clarity in discussing the model results, the laboratory angle $\theta + \phi$ is used instead, which is the angle between the molecular axis and the surface. These quantities are mathematically interchangeable upon proper substitutions. A variety of ranges for the molecular axis orientation of XeF are investigated, and it is found that a range of $-30° \leq \theta + \phi \leq 210°$ generates the best fit of the simulated F atom distributions to the measured TOF and angular distributions of the scattered F atoms, as shown in more detail below. The probability of having any orientation within this range is isotropic, meaning that any orientation is equally likely and therefore is equally represented in the simulated results. These probabilities are represented as

$$I(\theta + \phi) = 1 \quad \text{for} \quad -30° \leq \theta + \phi < 210° \quad \text{and}$$
$$I(\theta + \phi) = 0 \quad \text{for} \quad -30° > \theta + \phi \geq 210°. \quad (12)$$

Physically, this range of molecular orientations means that initial conditions with the F end of the XeF molecule pointing away from the surface and within ±120° from the normal are included in the simulation, and conditions with the F end pointing toward the surface and within ±60° of the nor-

mal are not. Inclusion of the latter molecular orientations leads to predictions of slower F atoms than observed. As discussed below, the XeF orientations with the F end pointing toward the surface and within ±60° of the normal are believed to be those that contribute to two atom abstraction.

The simulated spectra using the best fit functional forms for $I(E_{cm})$ and $I(\theta+\phi)$ in Eqs. (11) and (12) are plotted as solid lines in Fig. 3 along with the measured spectra (open circles) and the accompanying fit of the spectra to a Maxwell–Boltzmann distribution (dashed lines). The simulated spectra at $\theta_d=15°$, 30°, and 60° are normalized to a single point of the spectrum at $\theta_d=15°$. Specifically, the simulated spectra are normalized to 1.05 times the maximum value of the Maxwell–Boltzmann fit to the F atom data at $\theta_d=15°$. A scaling factor of 1.05 reproduces the measured data within the statistical error for all scattering angles in the 0–0.22 ML range of F coverage.

The goodness of fit of the simulated spectra to the measured spectra is estimated by computing a χ^2 value comparing the normalized simulated spectrum to the Maxwell–Boltzmann distributions fit to the measured F atom spectrum. The quantity χ^2 is defined as

$$\chi^2 = \sum \left(\frac{I_F^{lab}(v_F^{lab}(v_{XeF}), \chi_F(\theta)) - I_F(v_F, \chi_F)}{\sigma} \right)^2, \qquad (13)$$

where the quantities $I_F^{lab}(v_F^{lab}(v_{XeF}), \chi_F(\theta))$ and $I_F(v_F, \chi_F)$ are the count rates of the normalized simulated spectrum and the Maxwell–Boltzmann fit to the F atom TOF distributions, respectively. The quantity σ, is the statistical error in the F atom TOF spectra shown in Fig. 3. To examine the robustness of the $I(E_{cm})$ and $I(\theta+\phi)$ distribution functions, χ^2 was calculated for a wide range of $\bar{E}_{cm}$ and molecular orientations. In Fig. 8, contours of χ^2 are plotted as a function of $\bar{E}_{cm}$ and the allowed range of $\theta+\phi$ for scattering angles of $\theta_d=15°$, 30°, and 60°. The allowed range of $\theta+\phi$ is defined as the total angular range of molecular orientations allowed to dissociate in the simulation, i.e., $-30° \le \theta+\phi < 210°$ represents an allowed range of 240°, $-90° \le \theta+\phi < 90°$ represents an allowed range of 180°, and $-90° \le \theta+\phi < 270°$ represents an allowed range of 360°. As seen in Fig. 8, values of $\bar{E}_{cm}$ around 3.9 kcal/mol yield minimum values of χ^2 for scattering angles of $\theta_d=15°$ and 30°. At $\theta_d=60°$, higher center-of-mass energies yield slightly smaller χ^2 values, but the χ^2 values are less sensitive to $\bar{E}_{cm}$ above 3.9 kcal/mol. Therefore, the value of 3.9 kcal/mol was selected as the value for $\bar{E}_{cm}$ that produced the best overall agreement with the spectra at all scattering angles. Similarly, the allowed range of molecular orientations, shown as the range of $\theta+\phi$, is selected as the value producing the best average results at all three scattering angles, 240°. Variation in the average energy of $I(E_{cm})$ affects the shape of the simulated TOF distributions more so than variation in the allowed range of $\theta+\phi$, while variation in the latter has a larger effect on the relative fluxes of F atoms scattered at $\theta_d=15°$, 30°, or 60°.

To illustrate the sensitivity of the simulated spectra to the parameter $\bar{E}_{cm}$, spectra simulated using values of $\bar{E}_{cm}=2.96$ and 5.18 kcal/mol at $\theta+\phi=240°$ are plotted in Fig. 9 along with the measured spectra for all three scattering angles.

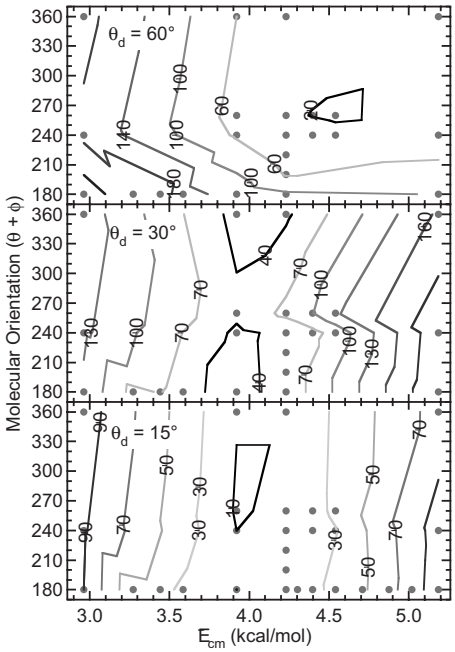

FIG. 8. Contours of χ^2 [Eq. (13)] are plotted as a function of $\bar{E}_{cm}$ and the allowed range of the molecular orientation, $\theta+\phi$, for scattering angles of $\theta_d=15°$, 30°, and 60°. The allowed range of $\theta+\phi$ is defined as the total angular range of molecular orientations allowed to dissociate in the simulation, i.e., $-30° \le \theta+\phi < 210°$ represents an allowed range of 240°, $-90° \le \theta+\phi < 90°$ represents an allowed range of 180°, and $-90° \le \theta+\phi < 270°$ represents an allowed range of 360°.

Clearly, decreasing $\bar{E}_{cm}=3.9$ by just 0.96 kcal/mol or increasing it by 1.26 kcal/mol results in visibly poorer agreement of the simulated spectra with the measured spectra. Similarly, spectra simulated using values of $\theta+\phi=180°$ and 360° at $\bar{E}_{cm}=3.9$ kcal/mol have been plotted in Fig. 10 along with the measured spectra for all three scattering angles. Once again, decreasing the range of $\theta+\phi$ by 60° or increasing it by 120° results in visibly poorer agreement with the measured spectra, particularly at short times in the TOF spectrum at $\theta_d=60°$.

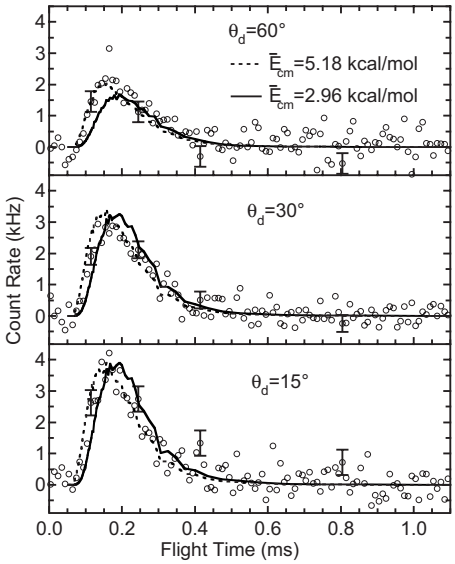

FIG. 9. Simulated F atom TOF spectra using values of $\bar{E}_{cm}=2.96$ (solid line) and 5.18 kcal/mol (dashed line) at $\theta+\phi=240°$ along with measured spectra for three scattering angles.

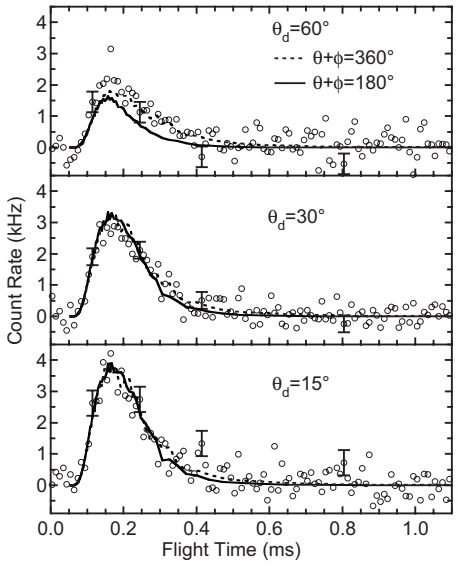

FIG. 10. Simulated F atom TOF spectra using values of $\theta+\phi=180°$ (solid line) and 360° (dashed line) at $E_{cm}=3.9$ kcal/mol along with measured spectra for three scattering angles.

Once the functions $I(E_{cm})$ and $I(\theta+\phi)$ are determined, they are used to predict F atom TOF spectra at $\theta_d=105°$, 120°, and 150°, which are angles where the F atom trajectories are aimed toward the surface, and hence where the scattered F atom flux cannot be measured. These spectra are simulated so that their velocity-weighted integrals over time, along with those of the spectra simulated at $\theta_d=15°$, 30°, or 60°, can be plotted versus scattering angle to yield a F atom angular distribution over both forward (away from the surface) and backward (toward the surface) scattering directions. The resulting simulated angular distribution, plotted as open circles, is plotted versus scattering angle, θ_d, in Fig. 4, along with the experimental flux measured at $\theta_d=15°$, 30°, or 60°. The simulated angular distribution is fit to a Gaussian function of the form

$$\Phi(\theta_d)=A\exp\left[-\left(\frac{\theta_d}{w}\right)^2\right], \tag{14}$$

where $\Phi(\theta_d)$ is flux, A is a scaling factor, and w is the width of the distribution in degrees. Although the flux was measured at only three scattering angles, the agreement between the measured and simulated angular distributions is reasonable. Note that values of $\theta_d>90°$ correspond to scattering of F atoms toward the surface.

The importance of simulating the F atom angular distribution over the entire range of scattering angles, even those angles that result in F atoms being directed toward the surface, lies in the need to determine the angle-integrated flux of F atoms. Knowledge of total F atom flux is necessary to impose conservation of mass on the Xe atom flux predicted by the simulation because for every F atom produced by a dissociation event, one Xe atom must be produced. That is, the total F atom flux is used to normalize the simulated Xe TOF spectra so that the predicted intensities of the Xe spectra can be compared to the measured Xe spectra as an additional test of the hypothesis that the F atoms arise from gas phase dissociation of XeF.

The total flux of F atoms, Φ_F, is calculated by integrating the Gaussian fit to the angular distribution, represented by Eq. (14), over all values of θ_d from −180° to 180° and all values of the out of plane, azimuthal scattering angle. The angular distribution is assumed to be symmetrical around the surface normal because XeF is produced by a reactive interaction and because its angular distribution, as well as those of the F and Xe atoms, are peaked at the surface normal. The same assumption is made in the integration of the Xe atom flux distribution to determine the total Xe atom flux.

In summary, the simulation results presented in this section show that the experimental TOF distributions of F atoms can be accurately fitted by physically reasonable functional forms of $I(E_{cm})$ and $I(\theta+\phi)$ [or equivalently, $I(\phi)$]. These functions are used in Sec. V B 2 to predict the scattered Xe TOF distributions based on a gas phase dissociation model for XeF.

2. Simulated Xe atom TOF

Once the functions $I(E_{cm})$ and $I(\phi)$ are optimized to accurately reproduce the F atom TOF and angular distributions, they are used to predict $I_{Xe}^{lab}(v_{Xe}^{lab},\chi_{Xe})$ using Eq. (10), the right hand equalities in Eqs. (6) and (7), the Newton diagram in Fig. 6 and the measured XeF velocity and angular distributions shown in Figs. 1 and 2. The simulation of Xe atom distributions uses the same number of trajectories as used in the simulation of F atom distributions. The intensities of the simulated Xe atom spectra are normalized such that the total number of Xe atoms integrated over all scattering angles is equivalent to the total number of F atoms in the simulated F atom spectra integrated over all scattering angles. This normalization procedure necessitates that the differences in the detection sensitivity of F and Xe be taken into account.

The procedure for normalizing the simulated Xe spectra to the angle-integrated F atom flux and for correctly accounting for the differences in the detection efficiency of F and Xe is as follows. The Xe atom TOF spectra simulated at six scattering angles, $\theta_d=15°$, 30°, 60°, 105°, 120°, and 150°, are integrated over time and the results are plotted versus scattering angle in Fig. 11. The angular distribution is fit to a single Gaussian function described by Eq. (14). The fit to the Xe atom angular distribution is then integrated over all scattering angles, as described for the integration of the F atom angular distribution, to obtain the total flux of Xe atoms, Φ_{Xe}, produced by the gas phase dissociation of XeF. Therefore, the intensity of the simulated Xe spectra is predicted on the basis of conservation of mass by multiplying each point of the raw simulated spectrum, $I_{Xe}^{lab}(v_{Xe}^{lab}(v_{XeF}),\chi_{Xe}(\theta))$, by the quantity

$$\left(\frac{\Phi_F}{\Phi_{Xe}}\right)\left(\frac{\sigma_{F\to F^+}}{\sigma_{Xe\to Xe^+}}\right)\left(\frac{T^{19}}{T^{129}}\right), \tag{15}$$

where $\sigma_{F\to F^+}/\sigma_{Xe\to Xe^+}$ is the ratio of cross sections for electron impact ionization at a specific electron energy of the designated species[23,13] and T^{19}/T^{129} is the ratio of the transmissions of the designated species through the quadrupole. The final two factors account for the relative detection efficiencies of Xe and F by the electron ionizer quadrupole mass

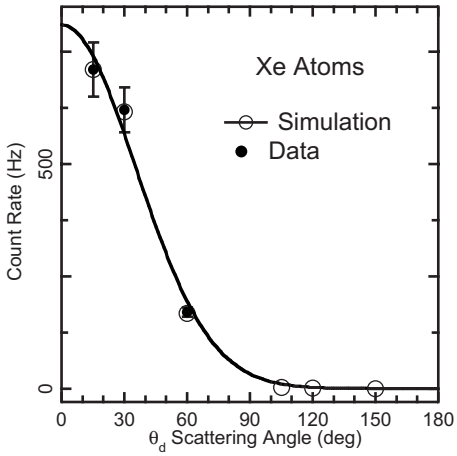

FIG. 11. Angular distribution of Xe flux produced by XeF dissociation. The flux at each angle is determined by time integration of the velocity-weighted counts of the simulated TOF spectra in Fig. 5. The solid dots represent count rates at scattering angles at which flux measurements are made. The open dots represent count rates at scattering angles at which only simulated results are possible. The line represents fit to simulated flux, Eq. (14).

spectrometer. The normalized simulated Xe atom velocity distribution is then transformed into a number density distribution in time and compared to the experimental spectra.

Shown in Fig. 5 are the results of the normalized Xe atom simulated spectra, plotted as lines along with the experimental spectra. The agreement between simulated and experimental spectra is excellent. At scattering angles of $\theta_d = 15°$ and 30°, where the contribution of Xe atoms from gas phase dissociation is the greatest, the simulation predicts Xe atoms at flight times where Xe atoms are observed. In particular, the simulation accurately predicts the rapid rise in the flux of fast Xe atoms at short flight times where comparison is most sensitive. Note that the simulated Xe intensities are not adjusted to fit the detected signal at $m/e=129$. Rather, they are predicted by the simulation using only $I(E_{cm})$, $I(\phi)$, and the relative values of the transmission functions and ionization cross sections of F and Xe. The error bars in the simulation (not visible on the scale of these figures) represent the uncertainty propagated from the determination of the transmission function and measured absolute ionization cross sections. The error is calculated to be 22% of the simulated intensity due mainly to the 20% uncertainty in the F atom ionization cross section.[23] The error bars on the data represent the statistical uncertainty, as described above. The quantitative agreement between experimental and simulated TOF spectra for the fastest Xe atoms is very strong evidence for gas phase dissociation of XeF, a gas phase product of a surface reaction.

While the simulated TOF spectra account for the Xe atoms that are observed at the shortest flight time and at scattering angles closest to the normal, they do not account for the entire Xe atom TOF distributions at $\theta_d=15°$ and 30°, nor the TOF spectrum measured at $\theta_d=60°$. This disagreement results not from a failure of the gas phase dissociation model but from the presence of two other channels for Xe atom production that are independent of gas phase dissociation. These channels are discussed in Sec. VII.

VI. DISCUSSION AND PHYSICAL CONSEQUENCE OF THE MODEL

A. Model assumptions

In the conversion of the F and Xe atom center-of-mass velocities to laboratory velocities, the model assumes that the velocity and angular distributions of the XeF molecules that dissociate are identical to those of XeF molecules that scatter intact. This assumption is necessary because the very short lifetime of the XeF molecules, as discussed in Sec. VI C, precludes their reaching the detector before they dissociate. The validity of this assumption is checked by comparing the fraction of XeF molecules above the dissociation energy as determined from the function $I(E_{cm})$ to the fraction of XeF that is measured to dissociate.

The function $I(E_{cm})$ in Eq. (11) and Fig. 7 show the distribution of XeF molecules with internal energy above the dissociation energy. The normalized distribution of XeF molecules with internal energies relative to the ground vibrational and rotational state is given by

$$I(E_{int}) = (RT)^{-1} \exp(-E_{int}/RT), \tag{16}$$

where $E_{int}=E_{cm}+3$ for a XeF bond dissociation energy of 3 kcal/mol.[7] Evaluation of this distribution function for the fraction of molecules with energies above the dissociation energy yields about 0.5 ± 0.1 for $RT=3.9\pm0.7$ kcal/mol. Hence, half of the XeF that is formed by F atom abstraction is predicted to dissociate in the gas phase. Recall that $I(E_{cm})$, and hence $I(E_{int})$, is determined solely by the measured F TOF distributions using the assumption that the velocity distribution of the dissociating XeF is identical to that of the intact XeF.

This value for the fraction of XeF predicted to dissociate is compared to the measured fraction of XeF that dissociates as given by

$$\frac{\Phi_F}{\left(\frac{\Phi_{XeF}}{0.4}\right)\left(\frac{\sigma_{F\rightarrow F^+}}{\sigma_{Xe\rightarrow Xe^+}}\right)\left(\frac{T^{19}}{T^{129}}\right)+\Phi_F}, \tag{17}$$

where Φ_{XeF} is the XeF flux that scatters intact as calculated by integrating the XeF angular distribution shown in Fig. 2, and 0.4 is the XeF cracking ratio to account for those XeF molecules that dissociatively ionize in the detector. The ionization cross section and transmission function for Xe are used as approximations to those of XeF. The fraction of XeF dissociation is thus calculated from the measured fluxes to be 0.9 ± 0.3. The large estimated error bars arise from the uncertainty in the probability of F ionization and XeF dissociative ionization in the detector. Within the uncertainties in the measurements, the prediction for the fraction of XeF that dissociates, 0.5 ± 0.1, is in agreement with the observed fraction of XeF dissociation, 0.9 ± 0.3. This agreement is reasonable validation of the assumption that the velocity and angular distributions of the intact and dissociating XeF are the same.

The right hand proportionality of Eqs. (8) and (9) shows that E_{cm} and ϕ are approximated as uncoupled. In principle, these variables need not be independent. Because the simu-

lated F atom TOF spectra matched the data to within statistical uncertainty, introduction of an additional parameter coupling E_{cm} and ϕ is not justified. The small amount of energy partitioned to the internal and translational degrees of freedom of XeF, relative to the available energy, is likely the origin of weak, if any, coupling between E_{cm} and ϕ.

The distribution of molecular orientations $I(\theta+\phi)$ that contribute to the F atom flux is assumed to be a step function, as shown in Eq. (12). That is, XeF molecular orientations with the F end of the XeF molecule pointing away from the surface and within $\pm 120°$ of the normal in the simulation can contribute to the F atom flux while XeF orientations with the F end pointed toward the surface and within $\pm 60°$ of the normal do not contribute. Realistically, the functional form of Eq. (12) is expected to be smooth because the strength of the attractive interaction between the F end of XeF and the surface is expected to vary gradually as a function of the XeF orientation. However, because the simulated TOF spectra match the measured data to within statistical uncertainty, no additional optimization of the functional form of Eq. (12) was possible.

Finally, the model predicts the intensity of scattered Xe atoms by setting the number of Xe atoms formed by dissociation of XeF to be exactly equal to the total number of F atoms produced, as described in the text leading to Eq. (15). However, about 2.5% of the Xe atoms have trajectories aimed toward the surface, as evident by the presence of Xe atom flux at scattering angles greater than $\theta_d=90°$ in Fig. 11. These Xe atoms interact with the surface a second time and either inelastically scatter or thermally desorb. Thus, these Xe atoms are not observed in the experiment with the characteristic velocity and angular distribution of the Xe atoms produced by gas phase dissociation. Because the percentage of these atoms is so small compared to the uncertainty (22%) in the predicted intensity, the inclusion of these trajectories is inconsequential to the analysis.

B. Partitioning of reaction energy to XeF

The energy E_{cm} is the vibrational and rotational energies partitioned to XeF and is the energy that provides the "kick" or kinetic energy with which the Xe and F atoms move away from each other. It is the internal energy relative to the XeF dissociation limit and is not the total internal energy partitioned to XeF. The total energy released to the internal degrees of freedom is measured relative to the ground vibrational and rotational states of XeF and its distribution is given by Eq. (16). Averaging this function over all energies yields a value of $\bar{E}_{int}=8.4$ kcal/mol. This average energy is the amount of available energy partitioned to the vibrations and rotations of the XeF abstraction product. Clearly, this amount of reaction energy partitioned, on average, into a diatomic product molecule with a bond strength of 3 kcal/mol leads to effective dissociation of the product, as observed in this experiment. Thus, the model's determination of $I(E_{cm})$ in Eq. (11) that, in turn, accurately predicts the angular and velocity distributions of the Xe atoms arising from gas phase XeF dissociation enables a detailed analysis of the partitioning of the abstraction reaction energy into the vibrational and rotational degrees of freedom, without the use of photon spectroscopic techniques.

Given that the total energy available to the reaction products is 69 kcal/mol and that the lowest lying electronic state of XeF, the $B(^2\Sigma_{1/2})$ state, lies 82.5 kcal/mol (Ref. 24) above the ground state, electronic excitation of XeF does not occur. However, an earlier calculation provided a value of 148 kcal/mol for the Si–F bond energy.[25] If this value were accurate, then the available energy is 83 kcal/mol and it becomes reasonable to ask whether excitation of the lowest electronic state of XeF might play a role in the dissociation mechanism. Electronic excitation requires, in this case, that all available energy be channeled into the *B* state. Once populated, the *B* state relaxes by photon emission to the ground state, leaving XeF in highly excited and nonbound rovibrational states of the ground electronic state that lead to dissociation. Alternatively, the *B* state intersystem crosses into the high lying and nonbound rovibrational levels of the ground electronic state. Electronic excitation is not considered operable here for two reasons. First, it is extremely unlikely for all available energy to be partitioned into a single degree of freedom, electronic excitation. Second, relaxation or intersystem crossing of the *B* state would result in very high rovibrational excitation of XeF, leading to a maximum of the $I(E_{cm})$ distribution far from zero energy, in contrast to the observation. Thus, given that relatively low internal energies used in the model fit well the measured F atom data, and that the model subsequently produces predictions of the scattered Xe atom velocity and angular distributions that agree with the measurements, it is concluded that electronic excitation of XeF plays no role in its gas phase dissociation even if the Si–F bond were as strong as 148 kcal/mol.

In addition to energy partitioning into the vibrations and rotations of the ground electronic state, energy is partitioned to the XeF translational degrees of freedom. The experimentally measured average translational energies are $\bar{E}_{trans}=11.6$, 10.1, and 8.4 kcal/mol for scattering at $\theta_d=15°$, 30°, and 60°, respectively, and are about equal to the average energy partitioned to the internal degrees of freedom. Adding this average internal energy to the average translational energies yields the total average energy partitioned to XeF from an atom abstraction event, $\bar{E}_{XeF}=20.0$, 18.5, and 16.8 kcal/mol at scattering angles of $\theta_d=15°$, 30°, and 60°, respectively. This total average energy represents 29%, 27%, and 24%, respectively, of the total energy available to the reaction products, where the total energy is the reaction exothermicity (67 kcal/mole) plus the incident energy (2 kcal/mol). The relatively low percentage of energy partitioned to XeF implies that the majority of the total available energy, about 50 kcal/mol, is partitioned to the vibration of the newly formed F–Si bond, as discussed in Sec. IV. As demonstrated in our previous work, this large energy release does not disorder the surface, implying that the energy in the newly formed F–Si bond effectively and rapidly flows into the surrounding large bath of Si surface vibrational modes.[12]

C. Nature of XeF dissociation

Given that the available reaction energy is channeled into the rovibrational continuum above the dissociation energy of the ground electronic state, the XeF fragment dissociates within a single vibrational period. Using the harmonic approximation to the fundamental frequency of the XeF vibration (225.40 cm^{-1}) (Ref. 7) and the measured average velocity of XeF (775 m/s), dissociation occurs within 2 Å of the transition state. Remarkably, even at this proximity to the surface, the XeF dissociation is successfully modeled as a gas phase process.

Because dissociation occurs within a single vibrational period and because the vibrational period is an order of magnitude shorter than the rotational period, XeF does not rotate away from its bond axis orientation in the transition state before it dissociates. The absence of rotation is supported by the fact that the measured F atom TOF data are best fit when the range of XeF molecular orientations is constrained between $\pm 120°$ from the surface normal, where 0° is defined as the XeF axis normal to the surface with the F atom end farther from the surface than the Xe atom end. That is, only these XeF orientations contribute to the F atom signal. Orientations of the XeF transition state where the F atom end is closer to the surface are more likely to react to form a second Si–F bond by a second two atom abstraction event and thus, do not contribute to F atom signal. Two atom abstraction is discussed in Sec. VII.

VII. TWO ATOM ABSTRACTION

A. Use of simulated Xe spectrum to quantify two atom abstraction mechanism

In addition to production of Xe atoms via gas phase dissociation of the vibrationally excited XeF product of the reaction of XeF_2 with Si, Xe atoms are produced by two atom abstraction. Two atom abstraction refers to reaction of the XeF product with the Si surface via a second F atom abstraction reaction, resulting in adsorption of both F atoms and production of a gas phase Xe atom. This pathway occurs when XeF does not escape the attractive interaction of the surface. That is, some XeF that is formed after the first F atom abstraction experiences a second F atom abstraction event and hence, does not scatter from the surface.

The XeF product molecules that likely undergo a second atom abstraction are those whose bond axis orientations have the F atom end pointed toward the surface. Molecules so oriented experience a much larger attractive interaction with the Si dangling bonds. The attractive interaction pulls the XeF molecule into the surface whereupon the F atom is abstracted, leaving the Xe atom to collide with the surface and eventually backscatter. This picture for the trajectories that undergo a second atom abstraction arises from the result that inclusion of XeF molecular orientations with the F end of the XeF molecule pointing toward the surface and within $\pm 60°$ of the normal in the simulation does not yield good agreement with the F atom TOF data. Their inclusion leads to predictions of slower F atoms than observed. Therefore, the XeF trajectories with the F end of the XeF molecule pointing toward the surface and within $\pm 60°$ of the normal are reasonably the ones that result in two atom abstraction and, hence, do not contribute to the F atom signal.

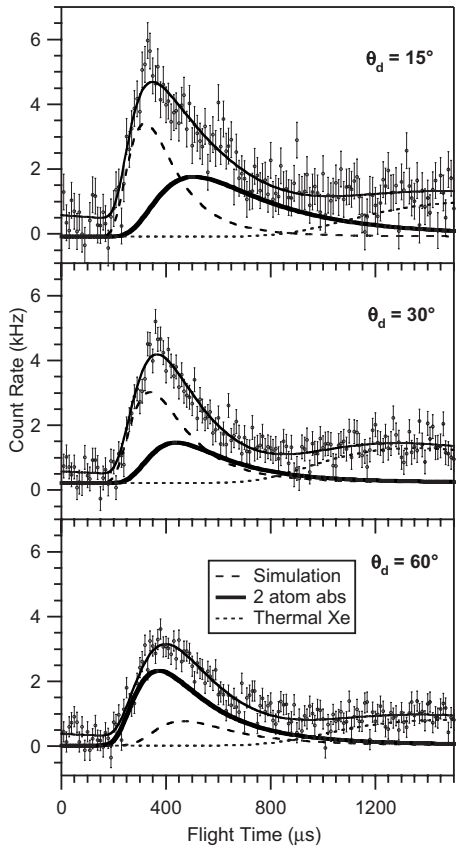

FIG. 12. Expanded flight-time scale of the net Xe atom TOF spectra shown in Fig. 5. Statistical error bar shown on each data point. The wide dashed line represents the simulated Xe spectra. The thick solid line represents inelastically scattered Xe atoms from two atom abstraction, while the narrow dashed line represents thermally accommodated Xe atoms from two atom abstraction. Thin solid line represents the sum of the simulated spectrum, the inelastically scattered Xe atom contribution and the thermally accommodated Xe atom contribution.

During or after the abstraction event, the Xe atom collides with the surface and may lose sufficient energy to be trapped. If so, the Xe atom equilibrates with the surface and eventually desorbs. The energy distribution of these Xe atoms is characterized by a Maxwell–Boltzmann distribution function with a mean energy of $2kT$, where T is the surface temperature. The corresponding distribution as a function of flight time is shown in Eq. (2). It is plotted, with T held at 150 K, as a narrow dashed line in Fig. 12. The parameters B, A, and t_f are adjusted to achieve the best fit. As is apparent, a Maxwell–Boltzmann distribution function at $T=150$ K describes well the energies of Xe atoms at the low energies of the distribution, demonstrating that some Xe atoms are indeed desorbing from the surface.

However, the Xe atom may not lose sufficient energy to be trapped when it collides with the surface during or after the abstraction event. In this case, the Xe atom scatters inelastically. These Xe atoms are apparent in Fig. 12 at flight times intermediate to those Xe atoms produced by XeF dissociation and those trapped Xe atoms produced by two atom adsorption. Their distribution is represented in Fig. 12 by a bold solid line and is obtained by the following procedure.

The measured Xe TOF distribution is fit to the sum of three distribution functions, corresponding to the three channels by which Xe is produced, and is shown as a thin solid line. One of those distributions is the result of the simulation, shown in Fig. 5, and is replotted in Fig. 12 as the wide dashed line. It represents the Xe atoms produced by XeF dissociation, which are the most energetic Xe atoms at $\theta_d = 15°$ and 30°. The parameters of this distribution and those of the thermal distribution at 150 K are held constant, while the parameters B, A, T, and t_f of the Maxwell–Boltzmann of the inelastically scattered Xe atoms are adjusted until the sum of the three distributions describe well the entire Xe atom TOF distribution. The resulting intensity of the distribution of inelastically scattered Xe atoms increases slightly as the scattering angle increases. The average energy of the inelastically scattered Xe atoms also increases from 5.3 ± 0.4 to 6.7 ± 0.6 to 9.5 ± 0.5 kcal/mol as the scattering angle is increased from 15° to 30° to 60°, respectively. These trends reflect the dynamics of the second atom abstraction event and are not investigated in detail here.

The ratio of two atom abstraction events that lead to inelastically scattered Xe atoms to those that lead to thermally accommodated Xe atoms can be evaluated from the angle-integrated fluxes of each contribution to the TOF spectra as follows. The Xe flux arising from the inelastically scattered events, as determined by integrating the distribution shown as a bold solid line in Fig. 12 over time, is plotted for each of the three scattering angles. The resulting angular distribution is fit to a cosine power function shown in Eq. (3) and integrated over scattering angle to yield the total angle-integrated flux of Xe atoms that are produced by inelastic scattering following a two atom abstraction event. An identical procedure is used to determine the total angle-integrated flux of Xe atoms that thermally accommodate after a two atom abstraction. The resulting ratio of inelastically scattered to thermally accommodated Xe atoms is 2. That is, it is twice as likely for Xe produced by two atom abstraction to scatter inelastically as for it to thermally accommodate in these experiments measured in the limit of zero F coverage. This ratio decreases dramatically as the F coverage is increased, as discussed in detail elsewhere.[17]

B. Branching ratio of XeF_2 reactivity: Single atom to two atom abstraction

Detection of gas phase dissociation of the XeF product and subsequent development of the model to describe the two-body dissociation are key to identification of all pathways in the reaction of XeF_2 with Si(100). These pathways include nonreactive scattering, characterized by scattering of intact XeF_2 from the surface, atom abstraction, characterized by both scattering of the XeF product and observation of F atoms and fast Xe created by XeF dissociation, and two atom abstraction, characterized by both inelastically scattered Xe and thermally accommodated Xe. It is clear from discussion and analysis of the Xe TOF spectra in Sec. V that Xe atoms produced with slower velocities by XeF dissociation overlap those produced by inelastic scattering after two atom abstraction so that resolution of the two pathways for Xe production for the purpose of determining branching ratios would not be possible without the model prediction developed here.

The ratio of the number of XeF_2 molecules that undergo single atom abstraction to produce intact or dissociated XeF to those that undergo two atom abstraction to produce an inelastically scattered or thermally desorbed Xe atom is determined in the following manner. The angular distribution of Xe flux, determined by time integration of the velocity-weighted counts of the simulated TOF spectra and shown in Fig. 11, is integrated over scattering angle to yield the total angle-integrated flux of Xe atoms produced by dissociation. This number is added to the total angle-integrated flux of intact XeF, determined from integration of the XeF angular distribution in Fig. 2, to yield the total flux of XeF produced by single atom abstraction. An identical procedure is used to determine the total angle-integrated flux of Xe atoms that inelastically scatter and thermally desorb following a two atom abstraction event. The result of this analysis reveals that $46 \pm 2\%$ of the XeF_2 that reacts does so via single atom abstraction, while $54 \pm 2\%$ reacts via double atom abstraction. The larger percentage of two atom abstraction reflects the ready availability of dangling bonds in these experiments in the limit of zero F coverage. This ratio is reversed as the F coverage increases.[17]

VIII. IMPLICATIONS FOR XeF_2 REACTIVITY

The model that accurately predicts the angle-resolved velocity distributions of the observed Xe atoms based on the observed F atom velocity and angular distributions also reveals that a small fraction of F atoms are not scattered into the gas phase but are scattered toward the surface. Figure 4 depicts both the model result for the F atom angular distribution and the experimental distribution. It can be seen that a portion of F atoms, those with scattering angles θ_d greater than 90°, are directed back toward the surface. This portion of the distribution, determined by integration over the intervals $90° \leq \theta_d \leq 180°$ and $-180° \leq \theta_d \leq -90°$ and over all values of the out of plane scattering angle, represents 9.2% of the total angle-integrated F atom flux. In the limit of zero F coverage, the conditions under which this experiment is carried out, these F atoms are captured by the dangling bonds. However at higher coverages where the availability of dangling bonds is scarcer, these F atoms react with Si–Si lattice bonds yielding SiF_2 and SiF_3 species that ultimately form volatile SiF_4. It is known that F atoms effectively etch Si.[26,27] Hence, the F atoms that are produced by gas phase XeF dissociation and are aimed back at the surface likely play a role in the dramatic difference in reactivity between F_2 and XeF_2.[12] The role of these backscattered F atoms is discussed in greater detail in a second paper.[17]

IX. SUMMARY

Xenon difluoride reacts with Si(100)2×1 by atom abstraction whereby a dangling bond abstracts a F atom from XeF_2, scattering the complementary XeF. Velocity measurements of the scattered XeF show that a small percentage of the available energy is partitioned into translation, consistent with an early barrier type of potential energy surface. How-

ever, a sufficiently large amount of the available energy is partitioned into rovibrational excitation of XeF to dissociate between 60% and 90% of the scattered XeF product within 2 Å of the surface. The angle-resolved velocity distributions of the F atoms are used to simulate the angle-resolved velocity distributions of the Xe atoms based on an energy, momentum, and mass conservation model. The simulation accurately predicts the flux and velocity of the fastest Xe atoms. This finding establishes that F and Xe atoms are produced by two body, gas phase dissociation of a product of a surface reaction, XeF. This observation is the first illustration of this type of chemical reaction mechanism and its discovery is attributable to the unique arrangement of the experimental apparatus and detailed analysis of the measured data.

The simulation model is also key to the quantitative identification of a second reaction pathway, two atom abstraction. It is found that some of the XeF product molecules do not scatter into the gas phase nor dissociate. Rather, those XeF molecules whose bond axis orientations at the transition state are within $\pm 60°$ of the surface normal with the F end pointed toward the surface undergo a second atom abstraction, resulting in adsorption of the second F atom and scattering of a gas phase Xe atom. About $54 \pm 2\%$ and $46 \pm 2\%$ of the incident XeF_2 reacts by two atom and single atom abstraction, respectively.

ACKNOWLEDGMENTS

This work was supported by the National Science Foundation under Contract No. CHE-0517786.

[1] Y. L. Li, D. P. Pullman, J. J. Yang, A. A. Tsekouras, D. B. Gosalvez, K. B. Laughlin, Z. Zhang, M. T. Schulberg, D. J. Gladstone, M. McGonigal, and S. T. Ceyer, Phys. Rev. Lett. **74**, 2603 (1995).
[2] R. C. Hefty, J. R. Holt, M. R. Tate, D. B. Gosalvez, M. F. Bertino, and S. T. Ceyer, Phys. Rev. Lett. **92**, 188302 (2004).
[3] S. T. Ceyer, D. J. Gladstone, M. McGonigal, and M. T. Schulberg, *Physical Methods of Chemistry*, edited by B. W. Rossiter and R. C. Baetzold, 2nd ed. (Wiley, New York, 1993), Vol IXA, p. 383.
[4] S. P. Walch, Surf. Sci. **496**, 271 (2002).
[5] M. P. D'Evelyn, Y. L. Yang, and L. F. Sutcu, J. Chem. Phys. **96**, 852 (1992).
[6] U. Hofer, L. Li, and T. F. Heinz, Phys. Rev. B **45**, 9485 (1992).
[7] P. C. Tellinghuisen, J. Tellinghuisen, J. A. Coxon, J. E. Velazco, and D. W. Setser, J. Chem. Phys. **68**, 5187 (1978).
[8] B. Itin, A. Bielecki, R. C. Hefty, J. R. Holt, R. G. Griffin, and S. T. Ceyer, (unpublished).
[9] D. P. Pullman, A. A. Tsekouras, Y. L. Li, J. J. Yang, M. R. Tate, D. B. Gosalvez, K. B. Laughlin, M. T. Schulberg, and S. T. Ceyer, J. Phys. Chem. B **105**, 486 (2001).
[10] M. R. Tate, D. Gosalvez-Blanco, D. P. Pullman, A. A. Tsekouras, Y. L. Li, J. J. Yang, K. B. Laughlin, S. C. Eckman, M. F. Bertino, and S. T. Ceyer, J. Chem. Phys. **111**, 3679 (1999).
[11] M. R. Tate, D. P. Pullman, Y. L. Li, D. Gosalvez-Blanco, A. A. Tsekouras, and S. T. Ceyer, J. Chem. Phys. **112**, 5190 (2000).
[12] J. R. Holt, R. C. Hefty, M. R. Tate, and S. T. Ceyer, J. Phys. Chem. B **106**, 8399 (2002).
[13] R. Rejoub, B. G. Lindsay, and R. F. Stebbings, Phys. Rev. A **65**, 042713 (2002).
[14] R. C. Hefty, Ph.D. thesis, Massachusetts Institute of Technology, 2004.
[15] Y. T. Lee, in *Atomic and Molecular Beam Methods*, edited by G. Scoles (Oxford University Press, New York, 1988), Vol. I, p. 553.
[16] J. R. Holt, Ph.D. thesis, Massachusetts Institute of Technology, 2002.
[17] R. C. Hefty, J. R. Holt, M. R. Tate, and S. T. Ceyer, J. Chem. Phys. (unpublished).
[18] M. R. Tate, Ph.D. thesis, Massachusetts Institute of Technology, 1999.
[19] M. G. Evans and M. C. Polanyi, Trans. Faraday Soc. **35**, 178 (1939).
[20] T. J. Chuang, Phys. Rev. Lett. **42**, 815 (1979).
[21] R. D. Levine and R. B. Bernstein, *Molecular Reaction Dynamics and Chemical Reactivity* (Oxford University Press, New York, 1987).
[22] Y. T. Lee and Y. R. Shen, Phys. Today **33** (11), 52 (1980).
[23] T. R. Hayes, R. C. Wetzel, and R. S. Freund, Phys. Rev. A **35**, 578 (1987).
[24] P. J. Hay and T. H. Dunning, Jr., J. Chem. Phys. **69**, 2209 (1978).
[25] C. J. Wu and E. A. Carter, J. Am. Chem. Soc. **113**, 9061 (1991).
[26] D. E. Ibbotson, D. L. Flamm, J. A. Mucha, and V. M. Donnelly, Appl. Phys. Lett. **44**, 1129 (1984).
[27] C. D. Stinespring and A. Freedman, Appl. Phys. Lett. **48**, 718 (1986).